RSC Advances

ROYAL SOCIETY OF CHEMISTRY

www.rsc.org/advances

Journal Name

ARTICLE

Synthesis and Electrochemical Performances of Mixed-Valence Vanadium Oxide/Ordered Mesoporous Carbon Composites for Supercapacitors

rReceived 00th October 20xx,
Accepted 00th October 20xx

DOI: 10.1039/x0xx00000x

www.rsc.org/

Liang Hao[a], Jie Wang[a], Laifa Shen[a], Jiajia Zhu[a], Bing Ding[a], and Xiaogang Zhang*[a]

Mixed-valence vanadium oxide (VO_x)/ordered mesoporous carbon (CMK-3) composites (VOC) were synthesized through a facile liquid-phase method followed by calcination. The microstructures of the composites were characterized by X-ray diffraction (XRD), nitrogen adsorption and desorption, X-ray photoelectron spectra (XPS), scanning election microscope (SEM) and transmission election microscopy (TEM). The relevant results showed that vanadium oxide nanoparticles with mixed valence were successfully embedded in mesoporous channels in the conductive matrix and dispersed on the CMK-3 surface to form the interwoven composite. The introduction of the CMK-3 framework not only improves electron transfer but also prevent the structure collapsing during cycling. As expected, the composite exhibits excellent electrochemical properties. It delivered a specific capacitance of 257 F g^{-1} at 0.5 A g^{-1} and maintained 77.3% at 8 A g^{-1} in 5 M $LiNO_3$. After 5,000 cycles, the capacitance only decreased 20%.

Introduction

With the social development and needs, efficient energy storage devices become increasing important in daily lives. Supercapacitors (SCs), one kind of the energy storage devices, have attracted great attentions due to their high power density, long cycle life, and low cost.[1-3] SCs can be classified as electrochemical double layer capacitors (EDLCs) and pseudocapacitors according to their charge storage mechanism.[4-5] Pseudocapacitors with high specific capacitance have been comprehensively investigated. Transition metal oxides (e.g., RuO_2[6], MnO_2[7], NiO[8], and Co_3O_4[9]) and conducting polymers (e.g., polyaniline and polypyrrole)[10-11] are the mostly used electrode materials for pseudocapacitors. Among them, vanadium oxides have been noticed to be a promising candidate electrode material for SCs owing to their high energy density and wide potential window, which can be attributed to the accessible layered structure and multiple stable oxidation states(V^{2+}, V^{3+} ,V^{4+} and V^{5+}). For example, V_2O_5 nanoporous network was reported to have a specific capacitance of 316 F g^{-1} in 0.5 M K_2SO_4 due to the interconnected network.[12] The hollow V_2O_5 spheres constructed from plate-like particles exhibited a high capacitance of 479 F g^{-1} at 5 mV^{-1} in 5M $LiNO_3$[13]. The 3D V_2O_5 nanosheets delivered energy density of 107 Wh kg^{-1} at a high power density of 9.4 kW kg^{-1}.[14] V_2O_5•0.6H_2O nanoribbons was prepared by a hydrothermal method. The nanoribbons were assembled an asymmetric supercapacitor with activated carbon and presented an energy density of 29.0 Wh kg^{-1}.[15] However, the low electrical conductivity and poor cycling stability of vanadium oxides restrict their application in electrochemical devices.[12] Several strategies have been employed to solve the issues, including nanocrystallization of vanadium oxides, doping with metal species and combination with carbon. The nanosized scales can significantly enhance the transport kinetics. Nanostructured the structure of vanadium oxides can shorten the ion and electron transport distances. Besides, the nanosized materials could increase the contact areas with electrolyte.[16] On the other hand, The combination of vanadium oxides and carbon was found to be an effective method to improve electronic transport.[17-25] V_2O_5/carbon nanotube core/shell hybrid aerogels exhibited excellent specific capacitance of 625 F g^{-1} in 1 M Na_2SO_4.[26] VO_2 nanobelts/reduce graphene oxide were prepared and it exhibited a specific capacitance of 769 F g^{-1} in 0.5 M K_2SO_4.[27] Graphene-bridge V_2O_3/VOx core-shell composite showed an exceptional discharge rate. When the scan rate increased to 50 V s^{-1}, it delivered a capacitance of 500 F g^{-1} in 1M Na_2SO_4.[28] The highly conductive carbon not only improves the conductivity and but also suppress the dissolution of vanadium oxides.[16, 29-30]

Ordered mesoporous carbon was considered as desirable electrode material in energy conversion and storage.[31] The CMK-3 materials with high conductivity, short-rod like morphology, and highly ordered pores have been reported to be an ideal host for electrode materials.[32-33] Yu et al[34] synthesized the V_2O_5/CMK-3 composites via a ultrasonic method. The composite exhibits a specific capacitance of 124 F g^{-1} in 1 M KNO_3. The double-layer capacitance of CMK-3 and

[a]Jiangsu Key Laboratory of Materials and Technology for Energy Conversion, College of Material Science and Engineering, Nanjing University of Aeronautics and Astronautics, Nanjing, 210016, P. R. China.

the pseudocapacitance of V_2O_5 enhanced the capacitance of the composite. Hu et al[35] prepared VO_2/CMK-3 composites by a solid-state reaction. The capacitance is higher than that of the pure CMK-3, owing to the pseudocapacitance of the VO_2. The channels in the CMK-3 matrix restrict the agglomeration and growth of vanadium oxide nanoparticles, shorten ion transport path. Furthermore, the high electronic conductivity of CMK-3 can enhance the conductivity of the composites, hence improving the rate capacity. However, in these reports, it is presented that the capacitances were enhanced by adding vanadium oxides to CMK-3 rather than the contrary.

The valence state of V has been proved to be important in the electrochemical performances of vanadium oxides.[36-39] In this work, highly ordered mesoporous carbon were firstly used to synthesize mixed-valence vanadium oxide (VO_x)/highly ordered mesoporous carbon composites through a facile liquid-phase method followed by calcination. The VO_x/CMK3 composite exhibits excellent electrochemical performance in 5M $LiNO_3$ electrolyte, achieving a capacitance of 257 F g^{-1} at 0.5 A g^{-1}; remaining 77.3% capacitance at a high current density of 8 A g^{-1}; only decaying 20% after 5,000 charge/discharge cycles. It has been demonstrated that being composited with CMK-3 is an effective method to increase the rate capacity and cycling life.

2. Experimental

2.1. Materials Synthesis

The short rod-like CMK-3 was synthesized by using SBA-15 with controlled morphology as hard template, which has been reported elsewhere.[33, 40] The VO_x/CMK-3 composites were prepared through a facile liquid-phase method followed by calcination. In typical, 150 mg Vanadyl acetylacetonate and 50 mg CMK-3 were dissolved in 100 ml ethanol with continuous stirring. Then the ethanol was removed by reduced pressure distillation. The resulting products were heated at 600 ^oC for 4 h with a ramping rate of 2 ^oC under a argon atmosphere. The final obtained VO_x/CMK-3 composites were denoted as VOC. For comparison, the sample without CMK-3 was also prepared through the same method. The resultant was denoted as VO_x.

2.2. Material Characterization

The structure was identified by X-ray diffraction (XRD), using Cu Kα radiation. The valence state of VOC was investigated by X-ray photoelectron spectroscopy (XPS) analysis, which was performed on a Perkin-Elmer PHI 550 spectrometer with Al Kα (1486.6 eV) as the X-ray source. Morphology was characterized by field emission scanning electron microscopy (FESEM, HITACHI S-4800) and transmission electron microscopy (TEM, JEOL JEM-2010). The specific surface areas (SSA) were calculated by the Brunauer-Emment-Teller (BET) method and the pore size distributions were derived from the adsorption branches of isotherms by using the Barrett-Joyner-Halenda (BJH) model through a Micromeritics BK122T-B analyzer.

2.3 Electrochemical Measurements

The electrochemical measurements including cyclic voltammetry (CV), galvanostatic charge-discharge (GCD) and electrochemical impedance spectroscopy (EIS) were performed on a CHI 660E electrochemical workstation in the 5 M $LiNO_3$ aqueous electrolyte. The sample electrode was prepared by pressed the slurry (contains 85 wt.% active material, 5 wt.% acetylene black and 10 wt.% polytetrafluoroethylene) onto 1 cm^2 stainless steel foam and dried at 80 ^oC for 12 h. The loading mass of the active material was 5 mg. The performance of the individual electrode was measured by a three-electrode cell system, in which platinum foil and saturated calomel electrode (SCE) were used as counter and reference electrodes, respectively. The specific capacitances (Cs) of the electrode were calculated from the galvanostatic discharge curves according to the equation:

$$C = \frac{I\Delta t}{m\Delta V}$$

where I (A) is the discharge current, Δt (s) is the discharge time, m (g) is the mass of the active material and ΔV (V) is the discharge potential window.

3. Results and discussion

Figure 1. Schematic illustration of the preparation of the VOC.

The preparation procedure of the VOC is presented in Figure 1.CMK-3 was impregnated in the ethanol solution of $VO(acac)_2$. The ethanol evaporate and the $VO(acac)_2$ was left in the channel or on the surface of CMK-3 because of the capillary action during the reduced pressure distillation process. When heated, the decomposition of $VO(acac)_2$ which was confined in the channels of the CMK-3 leads to form the VO_x/CMK-3 composites.

The XRD patterns of CMK-3, VOC and VO_x are shown in Figure 2. The small-angle XRD pattern of CMK-3 shows three scattering peaks which can be assigned to the (100), (110) and (200) reflections (Figure 2a), revealing a long range ordered mesoporous structures.[32] The diffraction peaks of (110) and (200) are not observed in VOC, suggesting that the ordered channels of CMK-3 are disarranged. In addition, the peak (100) shifted to higher angle compared to CMK-3, indicating pore-filling of the vanadium oxide nanoparticles blocked the mesoporous of CMK-3 partly.[41, 42] Figure 2b displays the wide-angle XRD patterns of CMK-3, VOC and VO_x. As for CMK-3, two broad diffraction peaks at 25^o and 43^{o}correspond to the (002) and (100) diffraction planes of graphite. In the case of VO_x, it shows four diffraction peaks at 27.7° , 37.1° , 42.3° and 55.5 ° , respectively, which can be indexed to the characteristic peaks of the VO_2 (JCPDS:44-0253). For the VOC, only one

broadness peak at 25° can be observed, which indicates poor crystallization and small crystallite size of the vanadium oxides.

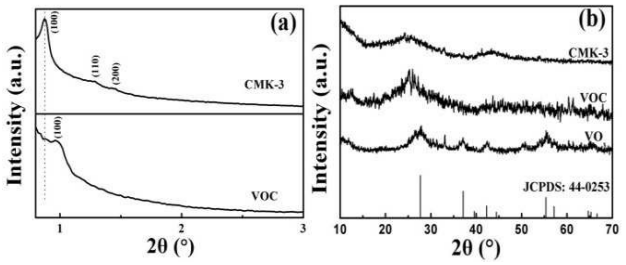

Figure 2.(a) Small-angle XRD patterns of CMK-3 and VOC. (b) wide-angle XRD patterns of CMK-3, VOC and VOx.

The short rod-like morphology and ordered porous channels of CMK-3 can be clearly observed in Figure 3a. The diameter of the CMK-3 rod is around 120 nm. The TEM images in Figure 3b exhibit the perfect ordered hexagonal arrangement of cylindrical mesoporous channels. The morphology of VOC is similar to that of CMK-3, suggesting that the structure can be remained after vanadium oxide filling (Figure 3c). The diameter of VOC is also about 120 nm, however, it's porous channels is not as clear as CMK-3. In addition, large vanadium oxide particles or aggregation was not observed, indicating that the vanadium oxide was completely embedded in the ordered channels or on the surface of CMK-3. The TEM image confirms that the ordered channels of CMK-3 are filled with vanadium oxide nanoparticles (Figure 3d). The size of vanadium oxide nanoparticles are estimated to be several nanometers. HRTEM was further carried out to investigate the microstructure of VOC (Figure 3d). The HRTEM image shows the lattice fringes with spacing of 0.21 nm, which corresponds to the (111) lattice plane of VO_2 (JCPDS:44-0253). The inset corresponding selected area electron diffraction (SAED) pattern indicate that the vanadium oxide in the VOC is polycrystalline. The diffraction rings ascribed to the (111) and (130) planes consistent with the structure of VO_2 (JCPDS:44-0253). In contrast, the bulk VOx aggregated severely together without CMK-3 during the synthesis process (Figure 3e).

BET method was adopted to further confirm that the vanadium oxide nanoparticles are embedded in the mesoporous channel of the CMK-3. In figure 4, both the CMK-3 and VOC present typical IV isotherm with clear H1 hysteresis loop, which is characteristics of mesoporous materials.[41, 43] The BET SSA, total pore volumes and pore diameters of CMK-3 and VOC are listed in Table 1. The BET surface area drastically decreases from 1233 $m^2\ g^{-1}$ of CMK-3 to 239 $m^2\ g^{-1}$ of VOC, indicating that the VO_x have filled in the CMK-3. Furthermore, the total pore volumes and pore diameters are 1.261 $cm^3\ g^{-1}$ and 4.465 nm for CMK-3, 0.081 $cm^3\ g^{-1}$ and 1.203 nm for VOC, respectively. The pore size distribution of CMK-3 centered at 4.5nm. However, the pore size distribution arranged form 1-4 nm present in the VOC. All these results support that vanadium oxides were embedded inside the pore channels of CMK-3.

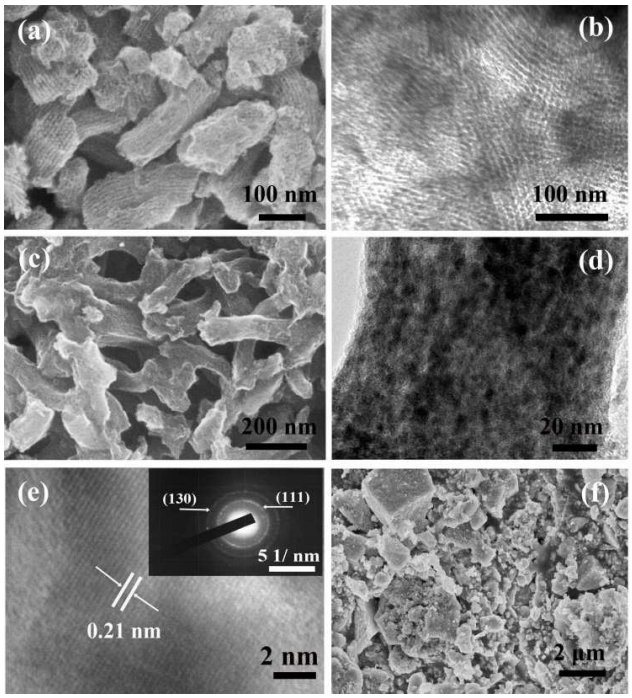

Figure 3.(a) SEM image and (b) TEM image of CMK-3,(c) SEM image and (d) TEM image of VOC, (e) HRTEM image of VOC and insert the corresponding SAED pattern, (f) SEM image of VOx.

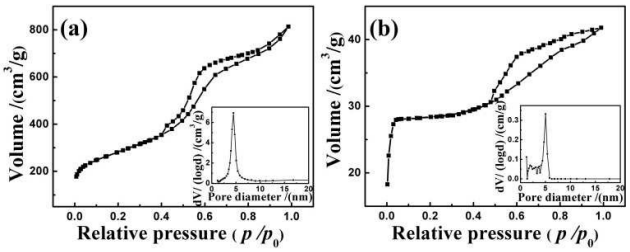

Figure 4.Nitrogen adsorption-desorption isotherms and insert the pore size distribution curves of CMK-3 (a)and VOC (b).

Table1 BET specific surface areas, total pore volumes and mean pore diameters of CMK-3 and VOC

sample	S_{BET} ($m^2\ g^{-1}$)	V_{pore} ($cm^3\ g^{-1}$)	D_{pore} (nm)
CMK-3	1233	1.261	4.465
VOC	239	0.081	1.203

To investigate the oxidation state of vanadium in the VOC, XPS analysis was carried out. The XPS survey spectrum in Figure 5a reveals that the VOC consists of carbon, vanadium and oxygen. The peaks centered at 284.7, 517.5, 525.0 and 530.5 eV are assigned to the C 1s, V 2p3/2, V 2p1/2 and O 1s, respectively. The high resolution C 1s spectrum shown was deconvoluted into three peaks (Figure 5b). The peaks at 284.7 eV, 285.8 eV and 288.9 eV are attributed to the assigning to C-C, C-OH and C=O groups. The O 1s spectrum can be assigned to the O^{2-} species in V-O (530.4 eV), OH^- group in H_2O molecule (531.5 eV) and superoxide ions O^-(533.5 eV)(Figure 5c). The V 2p3/2 peak is fitted by two peaks, corresponding to V^{5+} (517.6 eV) and V^{4+} (516.5 eV) while the V 2p1/2 peak is divided into two peaks corresponding to V^{5+} (525.1 eV) and V^{4+} (524.0

eV)(Figure 5d).The existence of V^{5+} in VOC is due to the inevitable oxidation of surface VO_2 .[19, 39, 44-46] The mass loading of VOx is 13.4% wt according to the XPS analysis.

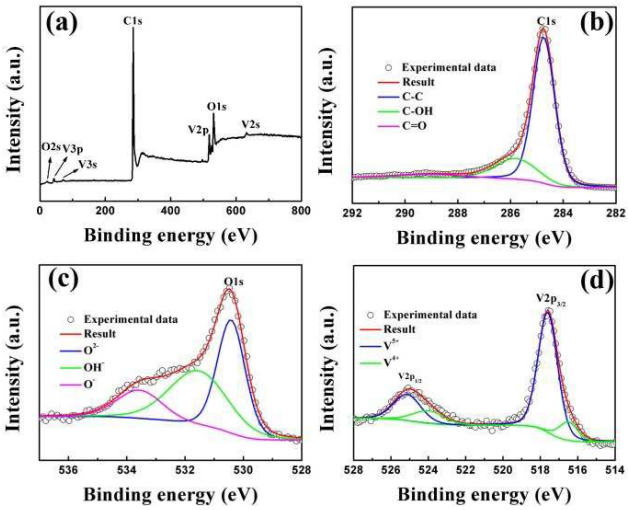

Figure 5. XPS survey spectrum of VOC surface (a), core level spectrum of C1s (b), O1s (c) and V2p (d) emanating from the sample.

The electrochemical performance was estimated through a three-electrode system in 5 M $LiNO_3$ electrolyte. The CV curves of VOC at different scan rates with the potential range from -0.9 to 0.6 V are shown in Figure 6a. When the scan rate increases to 20 mVs^{-1}, the CV curve still remains the similar shape, suggesting good rate capability of VOC electrode. The GCD measurements were also performed to estimate the specific capacitance. As shows in Figure 6b, two plateaus are observed in the curves revealing pseudocapacitive behaviour.[47] The performances of VOC show a combined characteristic of EDLCs and pseudocapacitor. In order to distinguish the contribution of EDLCs and pseudocapacitor, the CV curves were further analysed based on the work of Lu et al[48] and Perera et al[49]. The total voltammetric charge (Q_t) of the composite relies on the surface capacitive charge (Q_s) and diffusion-controlled charge (Q_d) which are responsible for the generation of electrical double layer and redox reactions, respecively:

$$Q_t = Q_s + Q_d$$

Assuming the Qs behaves linearly within the reasonable range of sweep rates, the following equation can be used to derive the charge components:

$$Q_t = Q_s + C\nu^{-1/2}$$

Figure 6c shows the relationship between total volumetric charge and the reciprocal square root of the sweep rate. Qs and Qd were reckoned by the fitted plot approximate values. Figure 6d exhibits the contribution of EDLCs and pseudocapacitor of the VOC. At 2 mV s^{-1}, some 50% of the charge storage comes from Qs, while at 20 mVs^{-1} it is 83%.

The CV curves of CMK-3, VO_x and VOC at the scan rate of 5 mVs^{-1} are shown in Figure 7a. The rectangular shape of the curves clear indicates EDLCs of CMK-3. However, for VO_x and VOC , two pairs of reversible redox peaks corresponds to the Li^+ insertion/extraction reactions of vanadium oxides can be observed.[4, 46] The cathodic and anodic peaks of VOC are much more obviously than that of the VO_x, indicating easier access of the electrolyte to the VOC. Furthermore, the area of the CV curves of VOC is larger than that of the VO_x, suggesting the preferable capacitor performance due to the addition of CMK-3.[50] The specific capacitance was calculated based on the discharge curves. The specific capacitance of VOC is 257 F g^{-1} at 0.5 A g^{-1}, which is higher than that of VO_x (218 F g^{-1}) and CMK-3 (143 F g^{-1}). The specific capacitances of CMK-3, VO_x and VOC as a function of the different current densities are compared in Figure 7b. At a high current density of 8 A g^{-1}, the specific capacitance of VOC electrode maintained 77.3% while the CMK-3 electrode maintained 74.8% and VO_x electrode only maintained 41.7%, verifying the improved the electro conductivity of the VO_x by introducing CMK-3. Besides, the electrical conductivity of VOC and VO_x are measured by four point probe. The electrical conductivity of VOC (0.23 S cm^{-1}) is higher than VO_x (0.01 S cm^{-1}), which leads to the good rate capability. Furthermore the surface defects V^{4+} and associated oxygen vacancies as well as less crystallized vanadium oxide can improve lithium ion intercalation capacity and electrical conductivity.[51-53]

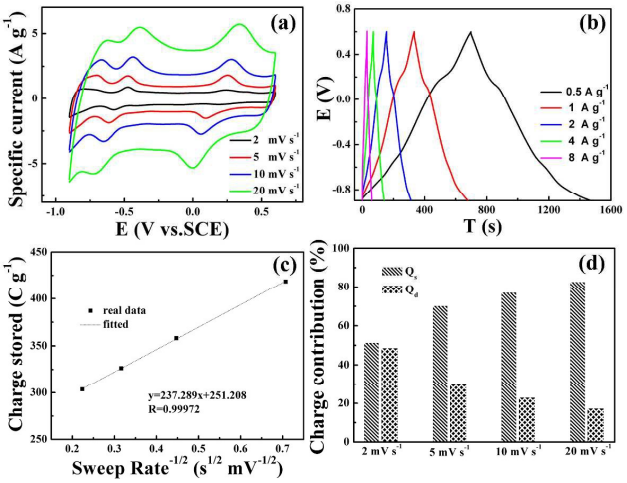

Figure 6.(a) CV curves of VOC at different scan rates. (b) Galvanostatic charge-discharge curves of VOC at different current densities. (c) charge stored versus the reciprocal of the sweep rate$^{-1/2}$ relationship for VOC. (d) Surface (Q_s) and diffusion (Q_d) charge contribution of VOC at different scan rates.

The high specific capacity and rate performance is highly related to the electric/ionic transport of electrode. EIS was performed to disclose the kinetic differences between VO_x and VOC (Figure 7c). High frequency region associated with semicircle reflects the combination of ohmic and charge transfer resistance of electrode material, and low frequency associated with straight line represents ion transportation resistance.[18, 30] An equivalent circuit (Figure 7c insert) is fitted to measure the impedance data, where R_s is internal resistance, C_{dl} is double layer capacitance, R_{ct} represents the charge

transfer resistance, W is Warburg impedance, and C_l is pseudocapacitance. The Rct value of VOC (4.3Ω) is lower than that of the VO_x (4.5Ω), indicating a decreased charge transfer resistance and improved lithium-diffusion rate. This could be attributed to the coupled with CMK-3. Cyclic performances was evaluated through GCD measurement at 1 A g^{-1} (Figure 7d) was recorded. The VOC exhibits good cyclic stability with the capacitance retention of ~ 80% after 5,000 cycles, which is much higher than that of VO_x (only 57.8% after 500 cycles). The results may be attributed to the agglomeration of vanadium oxide nanoparticles confined in the channels of the CMK-3 during cycling has been suppressed[32] and less crystalized structure.[53]

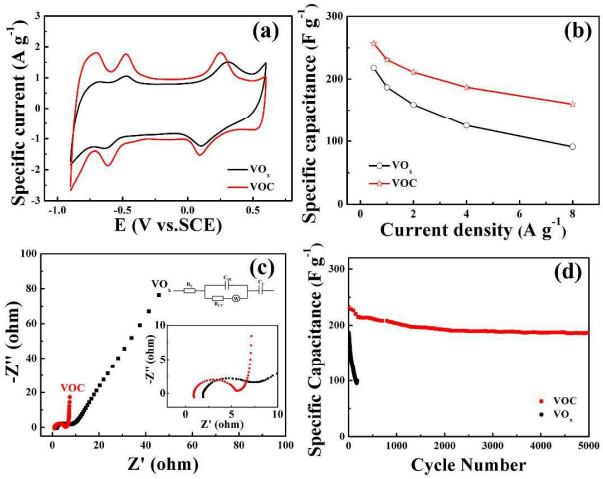

Figure 7.(a) CV curves of CMK-3, VO_x and VOC at 5 mv s^{-1}. (b) Specific capacitances calculated from galvanostatic charge-discharge curves with various current densities of CMK-3, VO_x and VOC. (c) Electrochemical impedance spectra of VO_x and VOC measured at the frequency range of 0.01 to 10^5 Hz. The inset shows the fitted electric equivalent circuit. (d) Cycling stabilities of VO_x and VOC. at 1 A g^{-1}

In short, the electrochemical performance of VOC is much higher than that of the VO_x, which could be attributed to: 1) the good electronic conductivity of CMK-3; 2) the high utilization of the nanostructured vanadium oxides; 3) the channels in the CMK-3 matrix improve the ion diffusion.

4. Conclusions

In general, mixed-valence vanadium oxide (VO_x)/ short rod-like mesoporous carbon (CMK-3) composites has been successfully obtained through a facile liquid phase method followed by calcination. The low valance state of V and the introduction of CMK-3 can enhance the electronic conductivity of the nanocomposite. Moreover, the CMK-3 can improve the cycling stability. The nancomposites exhibits a specific capacitance of 257 F g^{-1} at 0.5 A g^{-1} and maintained 77.3% at 8 A g^{-1} In addition its capacity retention decrease to 80% after 5,000 cycles. Therefore, the nanocomposite could be a promising electrode material for supercapacitors.

Acknowledgements

This work was supported by the National Basic Research Program of China (973 Program) (No. 2014CB239701), National Natural Science Foundation of China (No. 21173120, 51372116), Natural Science Foundation of Jiangsu Province (BK2011030), the Fundamental Research Funds for the Central Universities of NUAA(NP2014403).

Notes and references

1 P. Simon and Y. Gogotsi, *Nat. Mater.*, 2008, **7**, 845-854.
2 J. R. Miller and P. Simon, *Science*, 2008, **321**, 651-652.
3 Y. Gogotsi and P. Simon, *Science*, 2011, **334**, 917-918.
4 G. M. Wang, X. H. Lu, Y. H. Ling, T. Zhai, H. Y. Wang, Y. X. Tong and Y. Li, *ACS nano*, 2012, **6**, 10296-10302.
5 P. J. Hall, M. Mirzaeian, S. I. Fletcher, F. B. Sillars, A. J. R. Rennie, G. O. Shitta-Bey, G. Wilson, A. Cruden and R. Carter, *Energy & Environ. Sci.*, 2010, **3**, 1238-1251.
6 C. Z. Yuan, L. Chen, B. Gao, L. H. Su and X. G. Zhang, *J. Mater. Chem.*, 2009, **19**, 246-252.
7 G. H. Yu, L. B. Hu, M. Vosgueritchian, H. L. Wang, X. Xie, J. R. McDonough, X. Cui, Y. Cui and Z. N. Bao, *Nano Lett.*, 2011, **11**, 2905-2911.
8 C. Z. Yuan, X. G. Zhang, L. H. Su, B. Gao and L. F. Shen, . *Mater. Chem.*, 2009, **19**, 5772-5777.
9 F. Zhang, C. Z. Yuan, J. J. Zhu, J. Wang, X. G. Zhang and X. W. D. Lou, *Adv. Funct. Mater.*, 2013, **23**, 3909-3915.
10 Y. G. Wang, H. Q. Li and Y. Y. Xia, *Adv. Mater.*, 2006, **18**, 2619.
11 S. Biswas and L. T. Drzal, *Chem. Mater.*, 2010, **22**, 5667-5671.
12 B. Saravanakumar, K. K. Purushothaman and G. Muralidharan, *ACS Appl. Mater. Interfaces*, 2012, **4**, 4484-4490.
13 J. Yang, T. B. Lan, J. D. Liu, Y. F. Song and M. D. Wei, *Electrochim. Acta*, 2013, **105**, 489-495.
14 J. X. Zhu, L. J. Cao, Y. S. Wu, Y. J. Gong, Z. Liu, H. E. Hoster, Y. H. Zhang, S. T. Zhang, S. B. Yang, Q. Y. Yan, P. M. Ajayan and R. Vajtai, *Nano Lett.*, 2013, **13**, 5408-5413.
15 Q. T. Qu, Y. Shi, L. L. Li, W. L. Guo, Y. P. Wu, H. P. Zhang, S. Y. Guan and R. Holze, *Electrochem. Commun.*, 2009, **11**, 1325-1328.
16 X. Huang, X. H. Rui, H. H. Hng and Q. Y. Yan, *Part Part Syst Char*, 2015, **32**, 276-294.
17 Z. Chen, Y. C. Qin, D. Weng, Q. F. Xiao, Y. T. Peng, X. L. Wang, H. X. Li, F. Wei and Y. F. Lu, *Adv. Funct. Mater.*, 2009, **19**, 3420-3426.
18 M. L. Li, G. Y. Sun, P. P. Yin, C. Ruan and K. Ai, *ACS appl. Mat. & interfaces*, 2013, **5**, 11462-11470.
19 M. Lee, B. H. Wee and J. D. Hong, *Adv. Energy Mater.*, 2015, **5**.
20 J. Yang, T. B. Lan, J. D. Liu, Y. F. Song and M. D. Wei, *Electrochim. Acta*, 2013, **105**, 489-495.
21 C. H. Lai, C. K. Lin, S. W. Lee, H. Y. Li, J. K. Chang and M. J. Deng, *J. Alloys and Comp.*, 2012, **536**, S428-S431.
22 M. H. Bai, T. Y. Liu, F. Luan, Y. Li and X. X. Liu, *J. Mater. Chem. A*, 2014, **2**, 10882-10888.
23 H. Y. Li, K. Jiao, L. Wang, C. Wei, X. L. Li and B. Xie, *J. Mater. Chem. A*, 2014, **2**, 18806-18815.

24 D. H. Nagaraju, Q. Wang, P. Beaujuge and H. N. Alshareef, *J. Mater. Chem. A*, 2014, **2**, 17146-17152.
25 J. X. Zhu, L. J. Cao, Y. S. Wu, Y. J. Gong, Z. Liu, H. E. Hoster, Y. H. Zhang, S. T. Zhang, S. B. Yang, Q. Y. Yan, P. M. Ajayan and R. Vajtai, *Nano Lett.*, 2013, **13**, 5408-5413.
26 Y. J. Wu, G. H. Gao, H. Y. Yang, W. C. Bi, X. Liang, Y. R. Zhang, G. Y. Zhang and G. M. Wu, *J. Mater. Chem. A*, 2015, **3**, 15692-15699.
27 M. Lee, B. H. Wee and J. D. Hong, *Adv. Energy Mater.*, 2014, **5**.
28 X. Pan, G. F. Ren, M. N. F. Hoque, S. Bayne, K. Zhu and Z. Y. Fan, *Adv. Mater. Interfaces*, 2014, **1**.
29 G. L. Ye, Y. J. Gong, K. Keyshar, E. A. M. Husain, G. Brunetto, S. B. Yang, R. Vajtai and P. M. Ajayan, *Part. Part. Syst. Char.*, 2015, **32**, 817-821.
30 S. D. Perera, A. D. Liyanage, N. Nijem, J. P. Ferraris, Y. J. Chabal and K. J. Balkus, *J. Power Sources*, 2013, **230**, 130-137.
31 H. Jiang, J. Ma and C. Z. Li, *Advanced Materials*, 2012, **24**, 4197-4202.
32 L. Bingjiang, Z. Naiqing and S. Kening, *Small*, 2014, **10**, 2039-2046.
33 X. Ji, K. T. Lee and L. F. Nazar, *Nat. Mater.*, 2009, **8**, 500-506.
34 L. Yu, C. X. Zhao, X. Long and W. Chen, *Microporous and Mesoporous Mater.*, 2009, **126**, 58-64.
35 L. M. Hu, L. Yu, C. X. Zhao, X. Long and W. Chen, *J. Wuhan Univ. Technol.*, 2010, **25**, 574-578.
36 M. H. Yu, Y. Zeng, Y. Han, X. Y. Cheng, W. X. Zhao, C. L. Liang, Y. X. Tong, H. L. Tang and X. H. Lu, *Adv. Funct. Mater.*, 2015, **25**, 3534-3540.
37 T. Zhai, X. H. Lu, Y. C. Ling, M. H. Yu, G. M. Wang, T. Y. Liu, C. L. Liang, Y. X. Tong and Y. Li, *Adv. Mater.*, 2014, **26**, 5869-5875.
38 A. Altecor, Q. Li, K. Lozano and Y. Mao, *Ceram. Int.*, 2014, **40**, 5073-5077.
39 D. Zhao, L. R. Zheng, Y. Xiao, X. Wang and M. H. Cao, *ChemSusChem*, 2015, **8**, 2212-2222.
40 C. Yu, J. Fan, B. Tian and D. Zhao, *Chem. .Mater.* 2004, **16**, 889-898.
41 L. F. Shen, X. G. Zhang, E. Uchaker, C. Z. Yuan and G. Z. Cao, *Adv. Energy Mater.*, 2012, **2**, 691-698.
42 L. F. Shen, E. Uchaker, C. Z. Yuan, P. Nie, M. Zhang, X. G. Zhang and G. Cao, *ACS appl. Mater. interfaces*, 2012, **4**, 2985-2992.
43 G. X. Wang, H. Liu, J. Liu, S. Z. Qiao, G. M. Lu, P. Munroe and H. Ahn, *Adv. Mater.*, 2010, **22**, 4944-4948.
44 M. Shanmugam, A. Alsalme, A. Alghamdi and R. Jayavel, *ACS appl. Mater. interfaces*, 2015, **7**, 14905-14911.
45 G. Teran-Escobar, J. Pampel, J. M. Caicedo and M. Lira-Cantu, *Energy Environ. Sci.*, 2013, **6**, 3088-3098.
46 H. Q. Li, T. Y. Zhai, P. He, Y. G. Wang, E. Hosono and H. S. Zhou, *J. Mater. Chem.* 2011, **21**, 1780-1787.
47 T. Qian, N. Xu, J. Q. Zhou, T. Z. Yang, X. J. Liu, X. W. Shen, J. Q. Liang and C. L. Yan, *J. Mater. Chem. A*, 2015, **3**, 488-493.
48 Z. Chen, V. Augustyn, X. L. Jia, Q. F. Xiao, B. Dunn and Y. F. Lu, Acs Nano, 2012, 6, 4319-4327.
49 S. D. Perera, M. Rudolph, R. G. Mariano, N. Nijem, J. P. Ferraris, Y. J. Chabal and K. J. Balkus Jr, *Nano Energy*, 2013, **2**, 966-975.
50 C. W. Liang, D. Fang, Y. H. Cao, G. Z. Li, Z. P. Luo, Q. H. Zhou, C. X. Xiong and W. L. Xu, *J. Colloid. Interface Sci.*, 2015, **439**, 69-75.
51 C. Wu, F. Feng and Y. Xie, *Chem. Soc. Rev.*, 2013, **42**, 5157-5183.
52 M. Yu, Y. Zeng, Y. Han, X. Cheng, W. Zhao, C. Liang, Y. Tong, H. Tang and X. Lu, *Adv. Funct. Mater.*, 2015, **25**, 3534-3540.
53 D. Liu, Y. Liu, B. B. Garcia, Q. Zhang, A. Pan, Y.-H. Jeong and G. Cao, *J. Mater. Chem.*, 2009, **19**, 8789-8795.

TOC

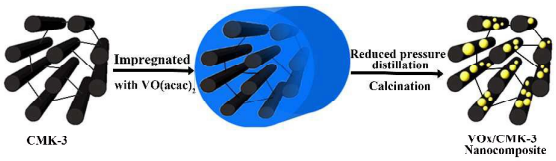

The highly ordered CMK-3 with short-rod like morphology significantly enhance the electrochemical performance of VO_x.